Phase diagram of Heisenberg fluids: Computer simulation and density functional theory

J. J. Weis
Laboratoire de Physique Théorique et Hautes Energies, Université de Paris XI, Bâtiment 211, F-91405 Orsay Cedex, France

M. J. P. Nijmeijer
Dipartimento de Fisica, Università degli Studi di Milano, via Celoria 16, 20133 Milano, Italy

J. M. Tavares and M. M. Telo da Gama
Departamento de Física da Faculdade de Ciências and Centro de Física da Matéria Condensada, Universidade de Lisboa, Avenida Professor Gama Pinto 2, P-1699 Lisboa Codex, Portugal

(Received 15 July 1996)

We have investigated equilibrium phases of a class of ferromagnetic Heisenberg fluids using computer simulations and a modified mean-field approximation. In the latter, configurations in the average of the perturbative part of the energy are weighted by the zero-density approximation of the pair distribution function. Although the theoretical results suggest a phase diagram with a tricritical point, the simulations provide some evidence for a magnetic critical point. Owing to finite size effects, however, the existence of a tricritical point cannot be ruled out. [S1063-651X(97)13901-0]

PACS number(s): 61.20.Gy, 64.60.Cn, 64.60.Kw, 64.60.Fr

I. INTRODUCTION

In a series of recent papers [1–3] we have investigated the phase diagram of a model ferrofluid, whose particles interact through two-body potentials consisting of a spherical hard-core and a Heisenberg-type interaction of their magnetic moments:

$$\phi(r,\vec{s},\vec{s}')=\begin{cases}\infty, & r\leqslant\sigma\\ I(r)+J(r)\vec{s}\cdot\vec{s}', & \sigma<r\leqslant r_c\\ 0, & r>r_c,\end{cases} \tag{1}$$

where σ is the hard-sphere diameter, r_c is a cutoff radius (assumed infinity in our earlier work), and $\vec{s}$ is a classical spin vector of unit length. In three spatial dimensions, the dot product in Eq. (1) may be written in terms of the angle α between $\vec{s}$ and $\vec{s}'$, or in terms of their azimuthal and polar angles, i.e., $\vec{s}\cdot\vec{s}'=\cos\alpha=\cos\theta\cos\theta'+\sin\theta\sin\theta'\cos(\phi-\phi')$. $J(r)$ and $I(r)$ are, respectively, the radial parts of the anisotropic and (soft) isotropic interactions [4].

Extensive mean-field (MF) calculations [5] have shown that the topology of the phase diagram depends sensitively on the relative strength of the isotropic and anisotropic interactions. Three types of phase behavior may be obtained depending on the ratio, R, of the integrated potentials $I(r)$ and $J(r)$,

$$R=J_{\rm int}/I_{\rm int}. \tag{2}$$

The theory predicts, in addition to isotropic liquid and vapor phases, a ferromagnetically ordered liquid phase, which is stable, at moderate to high densities. For weakly anisotropic potentials, the order-disorder transition is always continuous and terminates at a critical endpoint on (the liquid side of) the liquid-vapor coexistence curve. Increasing the anisotropy above a certain threshold drives the transition first-order at low temperatures, thus leading to the appearance of a tricritical point and a ferromagnetic liquid-isotropic liquid-vapor triple point. For strongly anisotropic potentials, ordinary liquid-vapor phase separation is preempted by a direct (condensation-ordering) transition between a low-density disordered phase and a ferromagnetic liquid, which becomes continuous at a tricritical point.

A system with $I(r)\equiv 0$ (or formally with $R=\infty$) has been previously studied in [1] by computer simulations. In what follows, we denote this system by the Heisenberg fluid. The liquid-vapor coexistence curve of the Heisenberg fluid was determined [1] from MC simulations, using the Gibbs ensemble method (GEMC) [6]. These calculations, for a system with 216 particles, were aimed at studying the full coupling, $J(r)$, i.e., $r_c=\infty$. In a simulation, however, the potential has to be truncated and thus a cutoff, equal to half the box length, was used; an estimate of the long-range contribution to the interaction energy was added to the simulation results. In the same work, the Curie line was located through canonical ensemble simulations, for a system with 500 particles. The average magnetization, $m=\langle|\vec{m}|\rangle=\langle|1/N\Sigma_{i=1}^{N}\vec{s}_i|\rangle$ (N number of spins) was recorded as a function of temperature, at two densities, $\rho^*=\rho\sigma^3=0.3$ and 0.7. The order-disorder transition temperature was estimated as the temperature where $m\approx 0.5$. It was concluded [1] that the Curie line intersects the coexistence curve at a critical endpoint, on the vapor side of the liquid-vapor coexistence curve. This scenario implies that, at temperatures above the critical endpoint, the phase diagram exhibits coexistence between a magnetic vapor and a magnetic liquid. This transition between two magnetic fluids ends, at a higher temperature, at an order-order critical point. If confirmed, this critical point is analogous to the solid-solid critical points investigated by Kincaid *et al.* [7] in studies of Ce and Cs, and by Frenkel and co-workers in studies of model colloids [8]. The simulation results for the Heisenberg fluid, however, appear

to be at variance with the results of MF theory [5], which does not predict this type of phase diagram for any *positive* value of the anisotropy ratio, R.

More recently [3], we have investigated the phase behavior of the ferromagnetic Heisenberg fluid using both MF and a more refined version of density-functional theory, viz., the modified mean-field approximation (MMF). In the latter, configurations in the average of the perturbative part of the energy are weighted by the zero-density approximation of the pair distribution function. This is known to yield an improved description of the liquid-vapor phase diagram of dipolar fluids [9]. Indeed, an overall improved description of the simulation results, for the system with $R=\infty$, is obtained within MMF theory [3]. Nevertheless, the theory still predicts that the phase diagram of this fluid exhibits a tricritical point [3], in (apparent) contradiction with the simulation results.

Clearly, small shifts in the simulated Curie line or the liquid-vapor boundary yield a phase diagram exhibiting a tricritical point rather than a critical endpoint. In view of the rough location of the Curie line, such shifts cannot be ruled out. In addition, it is not known how the liquid-vapor coexistence curve may be affected, close to (multi)critical points, by the rather small system size (216 particles).

In a subsequent paper [2], a more accurate location of the Curie line was obtained, by resorting to finite size scaling theory [10,11]. Simulations were carried out in the canonical ensemble at three densities, $\rho^*=0.7$, 0.6, and 0.4, for system sizes ranging from 108 to 1372 particles (2916 particles for $\rho^*=0.6$), at temperatures close to the transition temperature of the infinite system. The latter was determined from the intersection of the fourth order cumulants,

$$u_4=1-\frac{\langle m^4\rangle}{3\langle m^2\rangle^2}\,, \tag{3}$$

plotted as a function of temperature, for the different system sizes [10]. To obtain an accurate value for the intersection of the fourth order cumulants, advantage was taken of the histogram reweighting technique [12]. In addition, critical slowing down near the magnetic order-disorder transition was avoided by adapting the Wolff cluster algorithm, originally devised for lattice systems [13], to the continuum system under study. The model studied in these simulations differs from that of Ref. [1] by the truncation of the potential $J(r)$, at $r_c=2.5\sigma$; this is less than half the simulation box for all the system sizes, as required in order to apply finite size scaling arguments. Truncation of $J(r)$ affects quantitavely the phase diagram of the Heisenberg fluid. Indeed, MMF theory predicts that the tricritical temperature is lowered from $T^*_{\rm tc}=2.09$ to $T^*_{\rm tc}=1.39$, when the cutoff varies from infinity to 2.5σ [3]. The simulation of the liquid-vapor coexistence curve of the Heisenberg fluid, with a cutoff of 2.5σ, is thus required. This is one of the goals of this paper. As was done previously, the GEMC technique is employed. An estimate of finite size effects is also obtained by using systems with 512 and 1728 particles. In addition, an extra point on the Curie line is located. These simulation results are described in Sec. II.

In earlier theoretical work, we have searched for the coexistence of two orientationally ordered fluids for generalized Heisenberg models and found it, within mean-field theory, for a class of models characterized by *soft repulsive* isotropic interactions, in addition to the hard-core and ferromagnetic Heisenberg potentials [3]. These calculations were not confirmed by MMF theory and further investigation of this issue is the second goal of this paper. Although MMF theory is still approximate, it is expected to be more accurate than MF theory and thus the study of the global phase behavior of generalized Heisenberg fluid, based on MMF theory, may shed some light on the nature of the phase diagram of the simulated Heisenberg fluid. Indeed, if the order-order critical point is found to occur within MMF theory for values of the interactions closer to $R=\infty$ (when compared with the results of MF theory), then it is possible that the order-order critical point occurs in the Heisenberg fluid.

In this paper, we extend the calculations for the phase diagrams of generalized Heisenberg fluids to MMF theory and study the local stability of the tricritical point, for a wide range of parameters. These results are compared with those of MF theory. Unlike MF theory, where the topology of the phase diagram depends only on R, MMF theory is sensitive to the range of the interactions. We also investigate the effects of this range on the phase diagram of the model.

This paper is organized as follows. In Sec. II we present the simulation results. In Sec. III we sketch a derivation of the MMF approximation and compare the new phase diagrams with those found within MF theory. We carry out a Landau expansion for the MMF free energy, in order to obtain analytical conditions for the local stability of the tricritical point. Some details of these calculations are presented in the Appendix. Finally, in Sec. IV we make some concluding remarks.

II. SIMULATIONS

The liquid-vapor coexistence curve was determined using the GEMC technique. The method is now fairly standard and extensive descriptions are available in the literature [6]. Two system sizes were considered, with $N=512$ and 1728 particles, respectively. In each case, the N particles are distributed over two boxes with volumes V_1 and V_2, which fluctuate under the constraint of total fixed volume, V_1+V_2. At equilibrium, the pressure and chemical potential are the same in the two boxes. Table I collects the characteristics and the thermodynamic data (expressed in reduced units) of the vapor and liquid phases for the various runs, in the temperature range $T^*=kT/J=1.0-1.29$. The simulations were performed in cycles: one cycle consists of a trial displacement and rotation of the magnetic moment of every particle, one attempt to change the volume and $N_{\rm ex}$ attempts to exchange particles between the simulation boxes. As one of the boxes contains a ferromagnetic liquid, the efficiency of the insertion step was improved by the use of a bias: the spin orientation was chosen with a probability that favors orientations parallel to the local field, at the attempted (random) position [1,14]. This bias is, of course, accounted for in the acceptance probability of the particle transfer step. The acceptance ratios for the translation-rotation moves and volume changes were adjusted to lie in the range 30–50 %, while the value of $N_{\rm ex}$ was chosen to yield a success rate of particle transfers of 1–3 %, depending on the temperature. The (residual) chemi-

TABLE I. Details of the GEMC simulations.

			Vapor phase					Liquid phase				
kT/J	N	N_{cycles}	$\rho\sigma^3$	m	U/NkT	p/kT	μ'/kT	$\rho\sigma^3$	m	U/NkT	p/kT	μ'/kT
1.290	1728	400000	0.315(15)	0.44(2)	−0.85(5)		−0.318(3)	0.46(1)	0.76(1)	−2.07(4)		−0.314(3)
1.275	1728	154000	0.298(4)	0.41(2)	−0.77(4)		−0.346(4)	0.503(5)	0.797(5)	−2.45(4)		−0.342(6)
1.275	512	200000	0.288(5)	0.47(1)	−0.70(4)	∼0.41	−0.363(4)	0.504(5)	0.817(5)	−2.45(5)		−0.363(4)
1.250	512	80000	0.271(4)	0.32(2)	−0.59(4)	0.38(1)	−0.440(5)	0.533(8)	0.81(1)	−2.75(6)	0.40(2)	−0.441(8)
1.200	1728	230000	0.226(2)	0.140(3)	−0.368(4)		−0.674(5)	0.568(2)	0.844(1)	−3.21(2)		−0.678(5)
1.200	512	130000	0.230(2)	0.22(1)	−0.39(1)	0.329(5)	−0.66(1)	0.583(4)	0.850(2)	−3.34(3)	0.34(2)	−0.65(1)
1.111	512	180000	0.181(2)	0.12(1)	−0.29(1)	0.247(5)	−1.060(15)	0.665(3)	0.886(1)	−4.42(2)	0.21(2)	−1.071(15)
1.000	512	200000	0.114(1)	0.048(2)	−0.169(5)	0.137(2)	−1.80(1)	0.744(1)	0.914(1)	−5.84(1)	∼0.02	−1.79(1)

cal potential, $\mu'/kT=\mu/kT-\ln\Lambda^3$, was calculated during the insertion step using Widom's method, as generalized by Smit and Frenkel [15,16].

The pressure was calculated from the virial expression

$$\frac{p}{kT}=\langle\rho\rangle+\frac{p_{\text{HC}}}{kT}+\frac{1}{6kT}\left\langle\frac{1}{V}\sum_{\substack{i,j\\ i\neq j}}\left[-\vec{r}_{ij}\cdot\vec{\nabla}\phi_{ij}\right]\right\rangle, \qquad (4)$$

where p_{HC} is the hard core contribution. The spin part (third term on the right-hand side of 4) may be written as

$$\left(\frac{p}{kT}\right)_{\text{spin}}=-\frac{4\pi\rho_\alpha^2}{18kT}\int dr\; r^3J'(r)h_\Delta(r), \qquad (5)$$

where $J'(r)$ is the derivative of $J(r)$, $h_\Delta(r)$ is the projection of the pair distribution function on the spherical harmonic $\vec{s}\cdot\vec{s}'$, and ρ_α is the density of phase α. We note that, owing to the discontinuity of the potential at $r=r_c$, a δ-function contribution arises that is significant in the ferromagnetic phase only. It is given by

$$\left(\frac{p}{kT}\right)_c=\frac{4\pi\rho_\alpha^2}{18kT}r_c^3J(r_c)h_\Delta(r_c). \qquad (6)$$

Since, in order to save computer time, the pair distribution function was not calculated in the course of the simulations, we estimated the right-hand side of Eq. (6) by assuming that $h_\Delta(r)$ takes its asymptotic value, $h_\Delta(r)\to 3m^2$ $(r\to\infty)$, at the cutoff distance, $r=r_c$. The results of Table I show that, using this correction (6), the pressure of the liquid phase is in good agreement with that of the vapor, except at the lowest temperature, since in this case the correlation function has not reached its asymptotic value at $r=r_c$. The pressure of the system with 1728 particles was not calculated.

At the lowest temperatures studied, the surface tension is large and one of the boxes contains the vapor while the other contains the liquid phase. The histograms for density and magnetization exhibit two sharp peaks, corresponding to the two coexisting phases. An example is shown in Figs. 1 and 2, at $T^*=1.20$. In this case the densities and magnetizations, as well as the other thermodynamic functions at coexistence, were obtained as an average of the corresponding quantities in each box. Error estimates were calculated through block averages. For each property (density, magnetization) care was taken to choose the block size, larger than the decay ''time'' of the corresponding autocorrelation function (see, e.g., [17]).

When approaching the critical region the boxes were observed to switch identity near $T^*\simeq 1.275$, for the 512 particle system and near $T^*\simeq 1.29$, for the larger (1728) system. In this case the coexistence properties (densities, magnetiza-

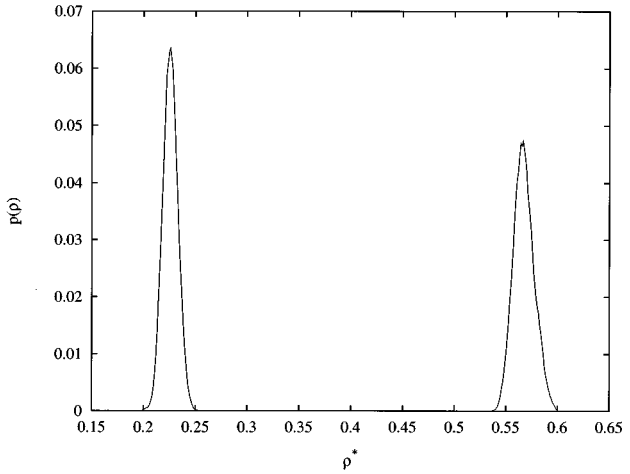

FIG. 1. Density distribution of the 1728 particle system at $T^*=1.20$.

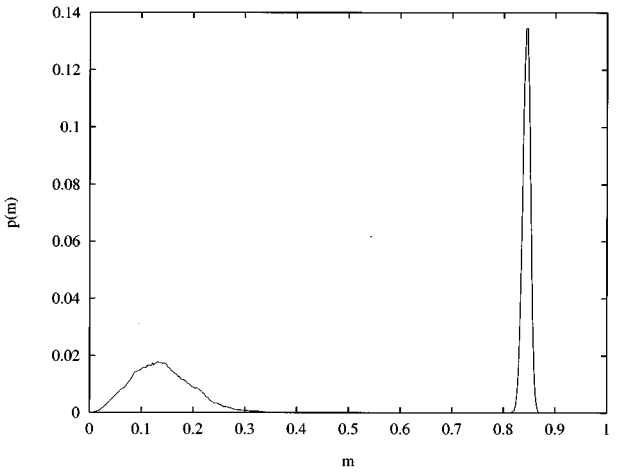

FIG. 2. Magnetization distribution of the 1728 particle system at $T^*=1.20$.

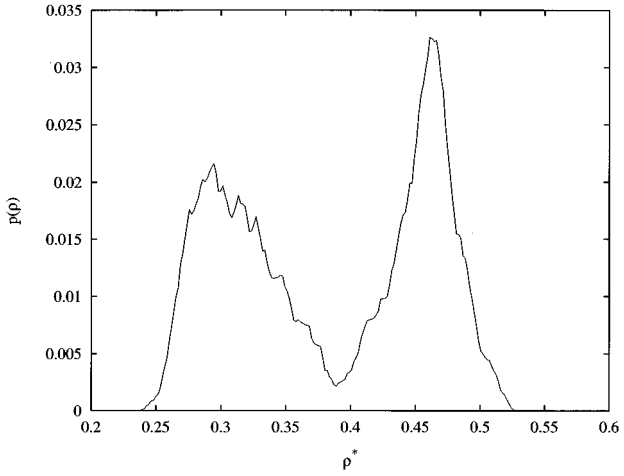

FIG. 3. Density distribution of the 1728 particle system at $T^*=1.29$.

tions) were obtained from the positions of the maxima of the corresponding histograms. However, density fluctuations are appreciable in the critical region, resulting in broad density distributions. This renders a precise location of the peak positions difficult. An example is shown in Fig. 3, at $T^*=1.29$ (1728 particles). For this state, the boxes switched identity three times, during 400 000 cycles (cf. Fig. 4, where the density in one of the boxes is plotted as a function of the number of MC cycles — note the rapid passage from one phase to the other). The average densities, calculated when the system is in a well defined phase in each box, are 0.299, 0.328, 0.302 for the vapor phase and 0.464, 0.466, 0.447 for the liquid phase. From these values, the average coexistence densities were found to be 0.31 ± 0.01 and 0.46 ± 0.01, compatible (within statistical errors) with those obtained from the peak positions of the density distribution function.

Finite size effects can be estimated for the temperatures $T^*=1.275$ and $T^*=1.20$, where two system sizes were considered. They are expected to be appreciable in the critical region only. In fact, no significant differences (within statistical error) were found at $T^*=1.275$, when the system size increases from 512 to 1728 particles. At the lower temperature $T^*=1.20$, however, we found a difference in the liquid coexistence densities, of 0.15, which is outside the combined error bars. Inspection of the density of the box containing the liquid phase (cf. Fig. 5) indicates that in this system the average density may not have converged after 200 000 cycles.

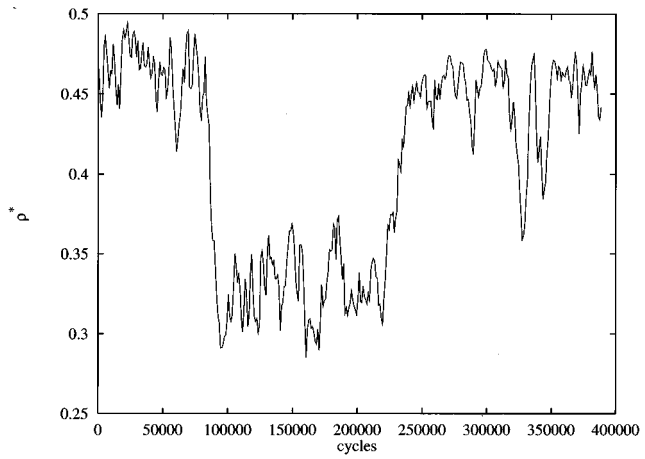

FIG. 4. Instantaneous density versus number of MC cycles of the 1728 particle system at $T^*=1.29$.

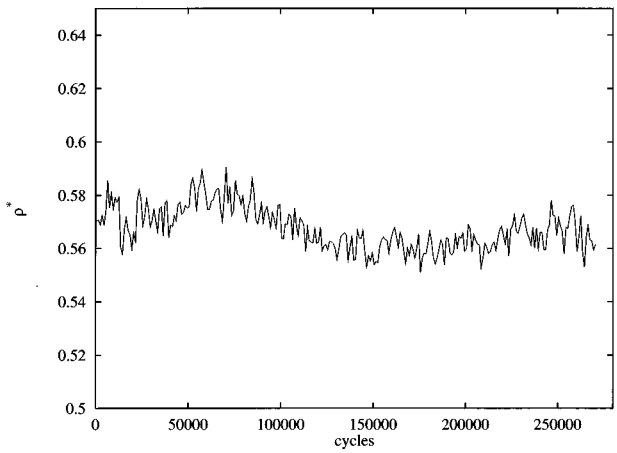

FIG. 5. Instantaneous density versus number of MC cycles of the 1728 particle system at $T^*=1.20$.

Results for the liquid-vapor coexistence curve and the Curie line are shown in Fig. 6 and in more detail in Fig. 7. The Curie line is obtained from canonical MC calculations of the order-disorder transition temperatures at four densities, $\rho^*=0.7$, 0.6, 0.4, and 0.31. The corresponding critical temperatures (for the infinite system) are $T^*=3.79\pm0.01, 3.150\pm0.005, 1.940\pm0.005$, and 1.442 ± 0.005, respectively. These were determined from the intersection points of the fourth order cumulants, u_4 [cf. Eq. (3)] plotted versus temperature, for different system sizes [10]. For the

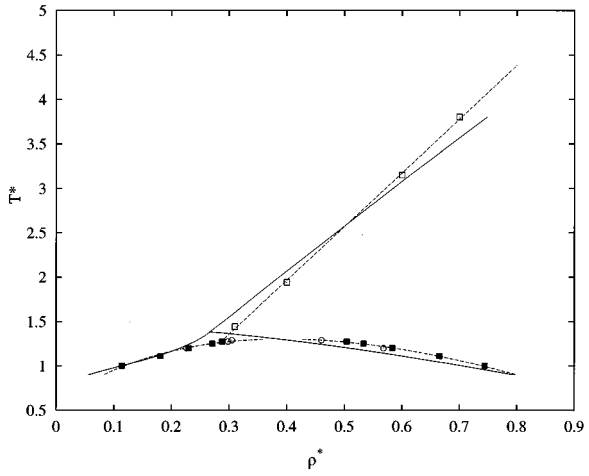

FIG. 6. Phase diagram of the ferromagnetic Heisenberg fluid. The open squares represent MC calculations of the Curie line. The filled squares (500 spins) and open circles (1728 spins) represent Gibbs ensemble MC data of the liquid-vapor coexistence curve. The solid lines are the modified mean field results from [3]. The dotted lines are fits to the MC data [a straight line for the Curie line, Eq. (7), with $\beta=1/2$ and the law of rectilinear diameters for the liquid-vapor coexistence curve]. They serve merely as a guide to the eye.

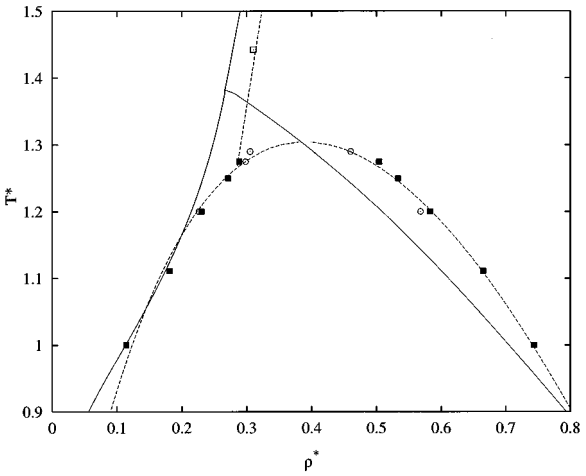

FIG. 7. Same as Fig. 6 (detail).

three highest densities, the system size ranged from 108 to 2916, while for the lowest density, three system sizes (108, 256, and 500 particles) were considered. The points for the three highest densities are from Ref. [2], where details of the calculations may be found. The point for $\rho^*=0.31$ is new. Over the temperature range considered in the simulations, the Curie line appears to be linear (within the uncertainty of the results).

We now address the question of whether the present simulation results allow us to discriminate between the situations described in the Introduction, namely, the Curie line ending at (i) a critical endpoint on the vapor side of the condensation phase boundary, as suggested by the early simulations, or (ii) a tricritical point, as suggested by the theory. In the vicinity of the critical (or tricritical) temperature, the density difference between the liquid and vapor phases (order parameter) (of a macroscopic system) vanishes with temperature, as

$$\rho_\ell-\rho_v\propto|T-T_c|^\beta, \tag{7}$$

where T_c is the critical (tricritical) temperature of the infinite system and β the bulk critical exponent. Equation (7) is valid only in the close neighborhood of the critical temperature. For a finite system, Mon and Binder [18] have shown that Eq. (7) has to be replaced by

$$\rho_\ell-\rho_v\propto|T-T_c(L)|^\beta, \tag{8}$$

if the correlation length ξ is less than the system size L, and that the behavior of the system crosses over to

$$\rho_\ell-\rho_v\propto|T-T_c(L)|^{\beta_{\rm eff}}, \tag{9}$$

when the correlation length ξ exceeds the linear dimension L of the simulation box. $T_c(L)$ is a size dependent critical temperature and the effective critical exponent, $\beta_{\rm eff}$, is given by its classical (mean-field) value, $\beta_{\rm cl}$. For sufficiently large systems, where the regime $\xi\ll L$ is established, the system will cross over from the behavior given by Eq. (8) to that described by Eq. (9), as the temperature approaches $T_c(L)$. In three-dimensional systems, however, this crossover may be difficult to observe.

If the three-dimensional Heisenberg model studied in this paper exhibits a tricritical point, the exponents take their classical, mean-field, values, since $d=3$ is the upper critical dimension for tricritical behavior [19]. These exponents depend on the path along which the tricritical point is approached as well as on the nature of the corresponding order parameter [19]. The number density, ρ, is a nonordering density and in this work the tricritical point is approached along the triple line, so that the corresponding critical exponent is $\beta=\beta_{\rm eff}=1$ [19].

It is readily seen, however, that Eq. (9), with $\beta_{\rm eff}=1$, does not yield a good representation of the simulation data, in particular, satisfying the requirement that the tricritical point is on the Curie line. We cannot rule out, however, that Eq. (9) applies only in a very narrow range of temperatures, near T_c. As remarked earlier, this region cannot be approached, reliably, by GEMC simulations. Another problem arises from the fact that the temperatures on the Curie line were calculated for an infinite system, while those of the first-order phase boundary correspond to finite system sizes. Although the difference between $T_c(L)$ and $T_c(\infty)$ is expected to be small, it may be relevant in this context.

The simulations appear to be compatible with an alternative scenario, as suggested by [1], i.e., the system exhibits an order-order (magnetic) critical point. In fact, a reasonable fit of Eq. (9) to the MC data, over the temperature range 1.1–1.29, is obtained, with $\beta_{\rm eff}\approx 1/2$. This is the mean field value of the coexistence curve exponent, for an ordinary critical point. In this case, the Curie line terminates on the coexistence curve, at a temperature close to $T^*=1.27$, and there is a small temperature region between $T^*=1.27$ and the order-order critical point, where the coexisting phases are a magnetized vapor and a magnetized liquid. With this picture in mind we have analyzed the variation of the magnetization along the coexistence curve. Along the liquid branch of the coexistence curve, the magnetization is well defined, varying from 0.91 at the lowest temperature to 0.76 at $T^*=1.29$ (cf. Table I). On the vapor side, the magnetization is very small at temperatures $T^*<1.25$, then increases to 0.32 at $T^*=1.25$, 0.41 at $T^*=1.275$, and 0.44 at $T^*=1.29$ (1728 particles). Fluctuations of the magnetization are important, as evidenced from the broad shape of the magnetization histogram (cf. Fig. 8). For $T^*\geqslant 1.25$, the coexisting vapor densities are close to the Curie line and finite size effects may play an important role. A more detailed study of the finite size effects is required before a definite conclusion is reached, as to the value of the infinite system magnetization, in this region. In particular, the expected nonclassical exponent for the three-dimensional Heisenberg fluid should be observed, before the crossover to the classical regime is obtained.

III. THEORY

A. Modified mean-field phase diagrams

Let us consider the generalized Heisenberg fluid of Eq. (1). Within density functional theory this system is characterized by the density orientational profile $\rho(\vec{r},\omega)\equiv\rho(\vec{r})\hat{f}(\vec{r},\omega)$, $\rho(\vec{r})$ being the density of particles at position $\vec{r}$ and $\hat{f}(\vec{r},\omega)$ the fraction of those particles with orientation $\omega\equiv(\theta,\phi)$. If the intermolecular potential ϕ is pairwise ad-

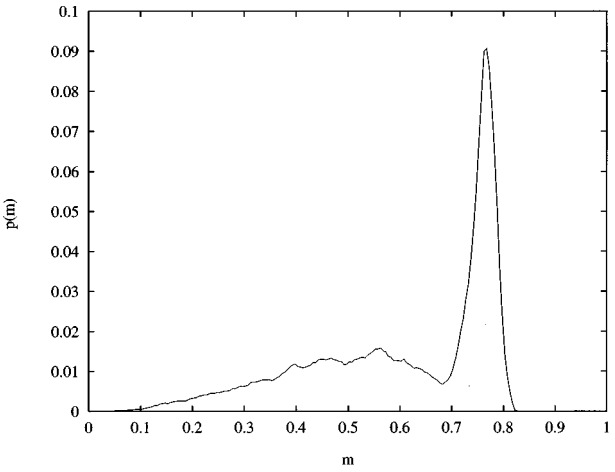

FIG. 8. Magnetization distribution of the 1728 particle system at $T^*=1.29$.

ditive and separable into a reference part ($\phi_{\rm ref}$) and a perturbation (ϕ_p), then [20] the free energy functional may be written as

$$\mathcal{F}[\rho(\vec{r},\omega)]=\mathcal{F}_{\rm ref}[\rho(\vec{r},\omega)]+\frac{1}{2}\int_0^1 d\alpha\int d\vec{r}_1 d\vec{r}_2 d\omega_1 d\omega_2 \times g(\vec{r}_1,\omega_1,\vec{r}_2,\omega_2;\alpha)\rho(\vec{r}_1,\omega_1) \times\phi_p(\vec{r}_1,\omega_1,\vec{r}_2,\omega_2)\rho(\vec{r}_2,\omega_2), \tag{10}$$

where $g(\vec{r}_1,\omega_1,\vec{r}_2,\omega_2;\alpha)$ is the pair correlation function of a system with interaction potential

$$\phi_\alpha(\vec{r}_1,\vec{r}_2,\omega_1,\omega_2)=\phi_{\rm ref}+\alpha\phi_p\,. \tag{11}$$

Equation (10) is exact but, in general, approximations are required in order to apply it to interacting systems.

We consider generalized Heisenberg fluids characterized by the potential of Eq. (1), and take for $J(r)$ the Yukawa form used in earlier work and for $I(r)$ the tail of the Lennard-Jones potential,

$$J(r)=-\epsilon_J\frac{\exp[-\lambda(r/\sigma-1)]}{r/\sigma}, \tag{12}$$

$$I(r)=-\epsilon_I\left(\frac{\sigma}{r}\right)^6. \tag{13}$$

The ratio R defined by Eq. (2) is now

$$R=\frac{\int_\sigma^{r_c} r^2 dr J(r)}{\int_\sigma^{r_c} r^2 dr I(r)} =\frac{3\epsilon_J}{\epsilon_I}\left[\frac{(1+\lambda)-(1+\lambda r_c/\sigma)\exp[-\lambda(r_c/\sigma-1)]}{1-(r_c/\sigma)^{-3}}\right]. \tag{14}$$

We consider ϵ_J greater than or equal to zero (ferromagnetic interactions only); R takes the sign of ϵ_I, which is positive for isotropic attractive interactions, and negative otherwise.

The reference part of Eq. (10) is treated as in [3], i.e., by using a local density approximation for the reference free energy functional and a random mixing approximation for the orientational entropy of a uniform, orientationally ordered fluid. The Carnahan-Starling free energy is used for the uniform hard sphere free energy density. The pair correlation function is approximated by a zero density approximation [21],

$$g(\vec{r}_{12},\omega_1,\omega_2;\alpha)=\exp(-\beta\phi_\alpha(\vec{r}_{12},\omega_1,\omega_2)). \tag{15}$$

Substitution of Eq. (15) into Eq. (10) yields the MMF free energy density of a uniform fluid:

$$\beta f(\rho,\{\eta_l\},T)=\beta f_{hc}-\frac{1}{2}\rho^2 u_0+\frac{1}{2}\rho^2\sum_{l=1}^{\infty} u_l\eta_l^2+\rho\,\ln\left(\frac{2}{C}\right), \tag{16}$$

where the coefficients u_l are found by integrating the perturbative part of Eq. (10),

$$u_l=4\pi\frac{2l+1}{2}\int_\sigma^{r_c} r^2 dr \times\left[\exp(-\beta I(r))I_{l+1/2}(t)\sqrt{\frac{2\pi}{t}}-2\delta_{l,0}\right]. \tag{17}$$

Here I_k is a modified Bessel function of order k, $t=|\beta J(r)|$ and the set $\{\eta_l\}$ denotes the coefficients of the expansion of $\hat{f}(\omega)$, in Legendre polynomials:

$$\hat{f}(\omega)=\sum_{l=0}^{\infty}\frac{2l+1}{4\pi}\eta_l P_l(\cos\theta). \tag{18}$$

C is a normalization constant given by

$$C=\int_{-1}^{1}\exp\left(\rho\sum_{k=1}^{\infty}\eta_k u_k P_k(x)\right)dx. \tag{19}$$

Minimization of Eq. (16), with respect to the order parameters η_l, yields their equilibrium values, which are the solution of the set of integral equations:

$$\eta_l=\frac{\int_{-1}^{1}P_l(x)\exp(\rho\Sigma_{k=0}^{\infty}\eta_k u_k P_k(x))}{C}. \tag{20}$$

We note that η_1 is just the earlier defined magnetization m.

Using Eq. (16), we find for the pressure (p) and the chemical potential (μ)

$$\beta p=\beta p_{hc}-\frac{1}{2}\rho^2\sum_{l=0}^{\infty}\eta_l^2 u_l, \tag{21}$$

$$\beta\mu=\beta\mu_{hc}-\rho u_0+\ln\left(\frac{2}{C}\right). \tag{22}$$

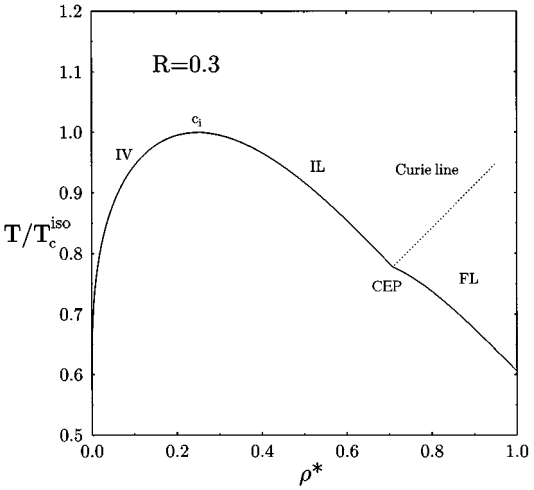

FIG. 9. Phase diagram of the Heisenberg fluid with $R=0.3$, in the MMF approximation (type I). T_c^{iso}, temperature of the isotropic critical point; FL, ferromagnetic liquid; IL, isotropic liquid; IV, isotropic vapor; full lines, first order phase transitions; dashed line, Curie line; c_i, isotropic critical point; CEP, critical end point.

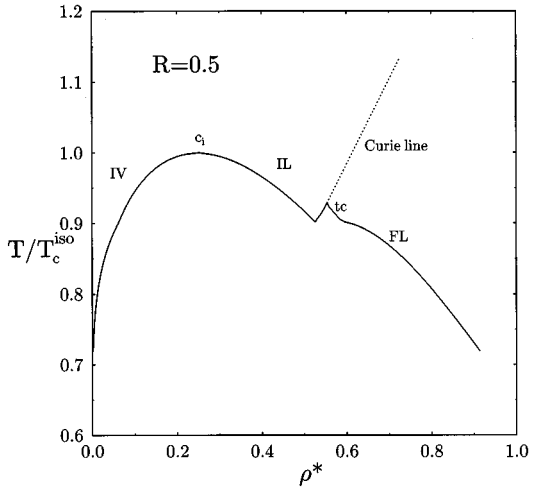

FIG. 10. Phase diagram of the Heisenberg fluid with $R=0.5$ in the MMF approximation (type II). tc, tricritical point.

At two-phase coexistence, the equilibrium densities are the solutions of

$$p(\rho_l,T)=p(\rho_v,T),$$

$$\mu(\rho_l,T)=\mu(\rho_v,T), \tag{23}$$

and the phase diagrams are calculated by solving Eqs. (23) and (20). For practical reasons, the sums over l are truncated at $l=6$ (see [3] for a discussion).

A systematic investigation of the MMF phase diagrams, as a function of R, was carried out. The existence of magnetic critical points, within the MMF approximation, has received particular attention, since it is significant in the context of the simulations described earlier. In Figs. 9–11 we plot the results for the MMF phase diagrams of three systems, with ''infinite'' r_c (in practice we took $r_c=10\sigma$) illustrating the different types of diagrams found, for positive R. A description of the phase transitions and critical points in each of these diagrams was discussed, in detail, in Sec. III of [3], so we just summarize it here. Three types of transitions were identified: a continuous order-disorder transition between ferromagnetic and isotropic dense fluids (Curie line), and two first-order condensation transitions. The temperature at which the Curie line meets the condensation phase boundary depends sensitively on R.

For weakly anisotropic fluids, the Curie line ends at a critical endpoint, CEP, on the condensation phase boundary. The corresponding temperature, T_{CEP}, separates a regime of isotropic liquid-vapor condensation from a regime of condensation-ordering transitions (Fig. 9, type I diagram). For stronger magnetic anisotropies, the critical end point becomes locally unstable and a tricritical point occurs at a temperature T_{tc}, where the Curie line terminates. The tricritical temperature increases with the anisotropy R, and this point separates two regimes of magnetic transitions. Above T_{tc} the magnetic transition is continuous (Curie line), while below, it is first order. This diagram also exhibits a triple point temperature T_{tr}, where a vapor, an isotropic liquid, and a magnetic liquid coexist (Fig. 10, type II diagram). As R increases, the triple point temperature also increases, until it becomes equal to the isotropic liquid-vapor critical point. At higher anisotropies, the isotropic critical point occurs at a temperature below T_{tr} and thus it is no longer globally stable (Fig. 11, type III diagram). This type of diagram persists up to $R=\infty$, i.e., for systems with no isotropic attractive interactions.

The tricritical point becomes locally unstable, at a negative value of R. At this point the system crosses over from tricritical behavior to a regime where an order-order critical point occurs (Fig. 12, type IV diagram). In these systems, the Curie line ends at a critical endpoint on the low density branch of the first-order phase diagram and, at temperatures between the critical endpoint and the magnetic critical point, phase coexistence occurs between two magnetic fluids.

Comparison of these results with those of Ref. [3] shows that for $R=0.3$ and $R=0.5$ we obtain the same type of phase diagrams within MF and MMF approximations. By contrast, for $R=0.7$ we obtain a phase diagram of type III within MF

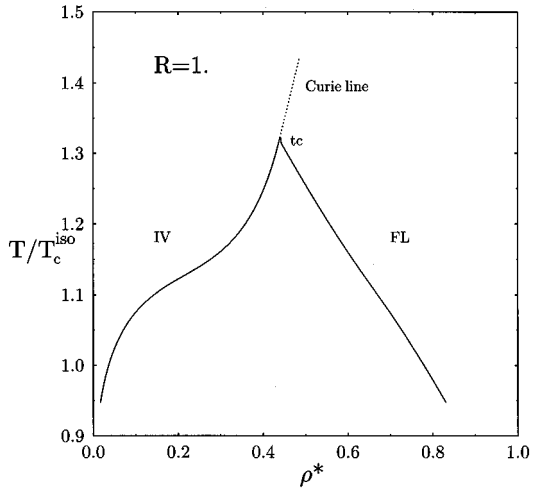

FIG. 11. Phase diagram of the Heisenberg fluid with $R=1$ in the MMF approximation (type III).

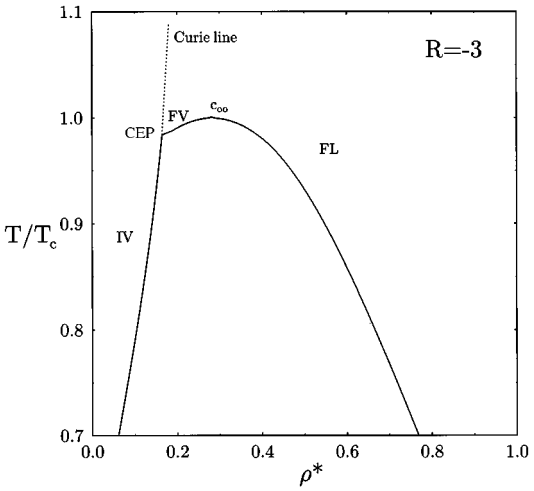

FIG. 12. Phase diagram of the Heisenberg fluid with $R=-3$ in the MMF approximation (type IV). c_{OO}, order-order critical point (OOCP). T_c, temperature of the OOCP.

theory while it is of type II using MMF (see the following subsection). This is an indication that MF theory overestimates the stability of the ordered phases (with respect to MMF theory) which results from neglecting correlations.

B. Stability of the tricritical point

A systematic comparison between MF and MMF approximations was carried out by calculating the values of R, where the type of phase diagram changes. These were calculated previously, within MF theory, by Hemmer and Imbro [5] who found, $R_{\text{I-II}}=0.38$ and $R_{\text{II-III}}=0.63$, and more recently by [3], who found $R_{\text{III-IV}}=-25.2$.

In order to calculate $R_{\text{I-II}}$ we require an equation for the tricritical point, since the transition from type I to type II is obtained, when T_{tc} equals T_{CEP} (see the preceding subsection). Likewise, the transition from type II to type III occurs when the triple point temperature equals the isotropic critical point and it is found by solving $T_c^{\mathrm{iso}}(R)=T_{\mathrm{tr}}(R)$. Finally, a phase diagram changes from type III to type IV when the tricritical point becomes locally unstable, i.e., when a ''tetracritical'' point appears [3].

Analytical expressions for the multicritical points referred to above were calculated using the MF free energy [3] by various methods. Here, we apply one of these to the MMF free energy. Briefly, the method consists in (i) calculating the MMF stability matrix, **M**, using Eq. (16); (ii) solving the stability equation, $\det\mathbf{M}=0$, in order to determine the critical points and the corresponding eigenvectors; (iii) expanding the free-energy in powers of a scalar parameter δ, about the critical point, along a direction parallel to a corresponding eigenvector. Details of these calculations are given in the next few lines and in the Appendix.

The elements of the stability matrix, **M**, are

$$M_{ij}=\frac{\partial^2\beta f}{\partial\rho_i\partial\rho_j}, \tag{24}$$

where $\rho_0=\rho$ and $\{\rho_i\}=\{\eta_i\}$ for $i\neq 0$. Local stability requires that the stability matrix is positive definite, i.e., that $\det\mathbf{M}>0$ [22]. This condition is first violated when $\det\mathbf{M}=0$. At continuous phase transitions, $\det\mathbf{M}$ vanishes on the phase boundary, i.e., at the critical point. There are two such solutions with $\{\eta_l=0\}(l\neq 0)$, corresponding to the isotropic critical point and to the Curie line. The latter is given by (see [3] and the Appendix)

$$\rho u_1=3, \tag{25}$$

and the corresponding eigenvector is

$$\mathbf{v}=(0,1,0\ldots). \tag{26}$$

Similarly, the condition for the tricritical point is obtained by expanding the free energy about one point on the Curie line, in the direction of **v**. We first consider variations (see also [23]) in ρ and η_i, about a point on the Curie line, of the type

$$(\rho,\eta_1,\eta_2,\eta_3,\ldots)=(\rho_{\mathrm{Curie}},0,0,\ldots)+(0,1,0,\ldots)\delta+(x_0,x_1,x_2,\ldots)\delta^2, \tag{27}$$

where $(x_1,x_2,\ldots)$ defines a line in density space which is, as yet, arbitrary. The corresponding variation in f is

$$\beta f(\rho,\{\eta_i\})=\beta f_{\mathrm{Curie}}+D(x_0,x_1,x_2,\ldots)\delta^4+O(\delta^5), \tag{28}$$

where D is given by

$$D(x_0,x_1,\ldots)=\frac{1}{2}\left(\frac{\partial^2\beta f_{\mathrm{HC}}}{\partial\rho^2}-u_0\right)x_0^2-\frac{3}{2}x_0+\frac{1}{2}\rho^2\sum_{k=2}^{\infty}\left(1-\frac{\rho u_k}{2k+1}\right)u_k x_k^2-\frac{3}{5}\rho^2 x_2 u_2+\frac{9}{20}\rho. \tag{29}$$

A tricritical point is obtained when D vanishes [3]. By minimizing D with respect to the x_i we find for $x_i^{\min}$

$$x_0^{\min}=\frac{3}{2\left(\frac{\partial^2 f_{\mathrm{HC}}}{\partial\rho^2}-u_0\right)}, \tag{30}$$

$$x_2^{\min}=\frac{3}{5\left(1-\frac{\rho u_2}{5}\right)}, \tag{31}$$

with $x_i^{\min}=0$ for $i>2$ and $x_1^{\min}$ arbitrary. A zero of $D_{\min}$ signals the onset of a local instability of the Curie critical point and yields the condition for tricriticality, i.e.,

$$\rho\frac{\partial^2\beta f_{\mathrm{HC}}}{\partial\rho^2}=\frac{5}{2}\left(\frac{3u_2-5u_1}{9u_2-5u_1}\right)+3\frac{u_0}{u_1} \tag{32}$$

is the equation for the tricritical points. This equation is the same as Eq. (7.24) of [24], which was obtained for dipolar fluids using MMF theory, and it is thus the general condition for tricriticality within the MMF approximation.

The condition for the local stability of the tricritical point may be obtained by writing a similar expansion for f, about a point on the tricritical line. This is done by considering variations of the type

$$(\rho,\eta_1,\eta_2,\ldots)=(\rho_{\rm tc},0,0,\ldots)+(0,1,0,\ldots)\delta+(x_0^{\rm min},x_1,x_2^{\rm min},\ldots)\delta^2, \quad (33)$$

which yields the expansion for f,

$$\beta f(\rho,\{\eta_i\})=f_{\rm tc}+E(x_0^{\rm min},x_2^{\rm min},\ldots)\delta^6+O(\delta^7). \quad (34)$$

The vanishing of the fifth order term in δ requires that $x_1=0$ and thus E depends only on $x_0^{\rm min}$ and $x_2^{\rm min}$. The tricritical point becomes locally unstable when $E=0$. In [3] this was referred to as a ''tetracritical'' point and it is the solution of

$$\frac{1}{6}\frac{\partial^3\beta f_{\rm HC}}{\partial\rho^3}(x_0^{\rm min})^3+\frac{1}{2}(x_2^{\rm min})^2x_0^{\rm min}\rho u_2\left(2-\frac{3}{5}\rho u_2\right)-\frac{1}{7\times15}(x_2^{\rm min})^3\rho^4u_2^3-\frac{3(x_0^{\rm min})^2}{\rho}-\frac{(x_2^{\rm min})^2\rho^5u_1^2u_2^2}{7\times15}-\frac{4}{15}x_0^{\rm min}x_2^{\rm min}\rho^3u_1^2u_2+\frac{9}{4}x_0^{\rm min}+\frac{2}{21\times15}x_2^{\rm min}\rho^6u_1^4u_2-\frac{9}{35}\rho=0. \quad (35)$$

$R_{\rm III\text{-}IV}$ is now obtained by solving simultaneously Eqs. (25), (32), and (35). These results were used to calculate the values of the anisotropy ratio where the phase diagrams change, within MMF theory.

TABLE II. Dependence of R on the cutoff, r_c (in units of σ). For cutoffs, $r_c<2.65$, the system of equations (25), (32), and (35) has no solution, and thus the OOCP does not occur. $R_{\rm III\text{-}IV}=-2.99$ when $r_c=2.65$.

r_c	$R_{\rm I\text{-}II}$	$R_{\rm II\text{-}III}$	$R_{\rm III\text{-}IV}$
10	0.43	0.71	−7.82
6	0.43	0.71	−7.63
4	0.42	0.69	−6.72
2.5	0.38	0.64	

We have obtained $R_{\rm I\text{-}II}$ for different values of r_c (ranging from 2.5 to 10, for $\lambda=1$) and found that $R_{\rm I\text{-}II}$ decreases slightly as r_c decreases (see Table II). Likewise we have calculated $R_{\rm II\text{-}III}$ for the same range of r_c, with $\lambda=1$, and found that $R_{\rm II\text{-}III}$ decreases weakly with r_c (see Table II). Finally, the value of $R_{\rm III\text{-}IV}$ was calculated as a function of r_c, for $\lambda=1$. We found that $R_{\rm III\text{-}IV}$ is always negative and that its absolute value decreases strongly with r_c. For values of $r_c<2.65\sigma$, a tetracritical point has not been found. This suggests that there is a threshold for the range of the interactions below which the type of condensation associated with the order-order critical point does not occur.

In addition, we have searched for a pair of values (r_c,λ) corresponding to a tetracritical point with $R=\infty$. This is relevant in the context of the simulations discussed previously. As noted before, for $\lambda=1$ we did not find a tetracritical point for any value of r_c when $R=\infty$. For values of $\lambda=0.01$, 0.1, 0.5, 2, 3, and r_c in the range $2<r_c<10$, we have also failed to find a tetracritical point for the Heisenberg fluid. This suggests that the tetracritical point and thus the possibility of an order-order critical point is associated with the change in sign of ϵ_I, i.e., with the inclusion of additional repulsions, at least within the MF and MMF approximations.

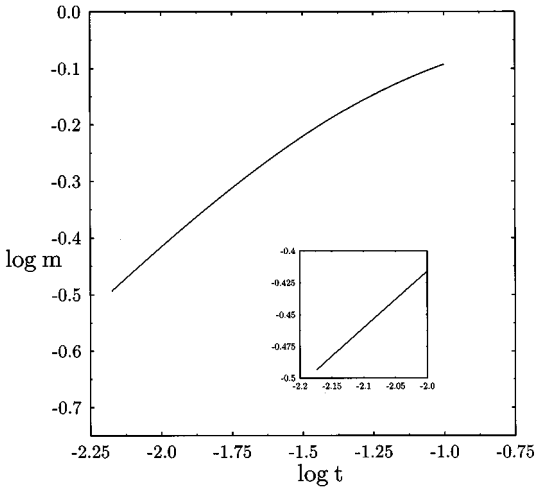

FIG. 13. MMF tricritical scaling region for the simulated Heisenberg fluid ($R=\infty$ and $r_c=2.5\sigma$). $\log_{10}m$ on the coexistence line vs $\log_{10}(1-T/T_{\rm tc})$. The scales were chosen so that, as the tricritical temperature is approached, the curve approaches a straight line parallel to the main diagonal, corresponding to $\beta=0.5$. This behavior is illustrated in the inset. The slope calculated from the two points closest to the tricritical temperature yields $\beta=0.456$.

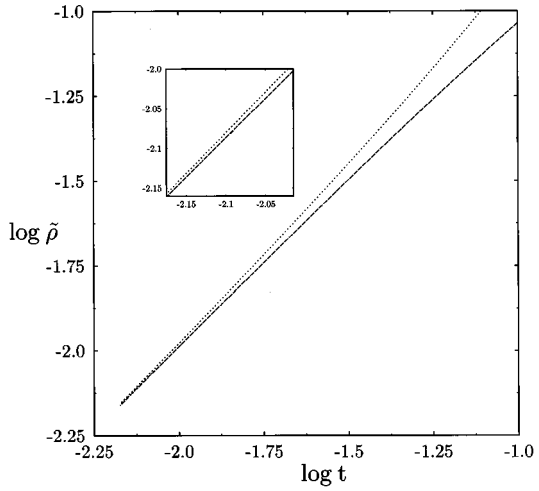

FIG. 14. MMF tricritical scaling region for the simulated Heisenberg fluid ($R=\infty$ and $r_c=2.5\sigma$). Dashed line, $\log_{10}(\rho_l/\rho_{\rm tc}-1)$; dotted line, $\log_{10}(1-\rho_v/\rho_{\rm tc})$. The dashed line was shifted by a constant for clarity. The scales were chosen so that on approaching the tricritical temperature the two curves approach a straight line parallel to the main diagonal, since $\beta_l=\beta_v=1$. This is shown in the inset. The slopes calculated from the two points closest to the tricritical temperature are $\beta_l=0.994$ and $\beta_v=1.019$.

IV. CONCLUSIONS

The results of MMF are expected to be closer to the exact results than those of MF theory. MMF is obtained from a ''zero-density'' limit of the pair correlation function and thus it must be reasonably accurate at low densities. At higher densities, we base our assumption on the fact that, for $R=\infty$, the MMF results are indeed closer to the simulation results (see [3]).

We have found that, at least for positive R, MF overestimates the anisotropic interactions (correlations), when compared with MMF. This is what we may have anticipated since MF theory is known to overestimate the stability of the ordered phases. In fact, a comparison of the values of $R_{\text{I-II}}$ and $R_{\text{II-III}}$ shows that more anisotropic interactions are required within MMF (larger R) to cross over from the weak to the strong magnetic regimes, in line with the above discussion. This is corroborated by the fact that for the same value of R, the ordered phase is more stable within the MF approximation.

The question still remains of whether an order-order critical point occurs for a system with $R=\infty$, within an ''exact'' calculation. If this is the case, we would expect the MMF $R_{\text{III-IV}}$ to be closer to infinity than the corresponding MF result. Or, in other words, we would expect that less isotropic repulsions are required in MMF than in MF theory. However, this is not what happens. In fact, $R_{\text{III-IV}}^{\text{MMF}}=-7.8$ (for $r_c=10$) while $R_{\text{III-IV}}^{\text{MF}}=-25.2$. Inspection of Table II also shows that this trend is even more pronounced for lower values of r_c, i.e., $|R_{\text{III-IV}}|$ within MMF is smaller for any other value of r_c. We cannot rule out that the MMF results are less accurate than those of MF theory, but at present we do not see why this should occur.

By contrast, the simulations reported in Sec. II do not provide conclusive evidence for either the tricritical or the order-order critical point scenario. We have calculated the size of the tricritical scaling region of the Heisenberg fluid within the MMF approximation and the results are summarized in Figs. 13 and 14. We note that ρ_v has a wider scaling region than either ρ_l or m. These results suggest that the simulation points may be outside the scaling region, except, perhaps for points on the vapor branch. However, in order to settle this issue we need an accurate estimate of $T_c(L)$. In the absence of this information we can only suggest that this is a problem.

More accurate theoretical results are unlikely to be obtained with current techniques, and thus the type of criticality of the Heisenberg fluid must be settled by further simulations. A possibility is the use of an approach similar to that adopted by Wilding and Nielaba [25] to investigate the tricritical point of a two-dimensional Ising spin fluid. These authors locate the tricritical point using the cumulant intersection method. The fourth order cumulants of the magnetization corresponding to various system sizes, intersect at a point which is the tricritical temperature. The possibility to apply a similar approach to the present three-dimensional Heisenberg fluid is under investigation.

ACKNOWLEDGMENTS

One of us (J.J.W.) acknowledges helpful discussions with D. Levesque and G. Stell. The Laboratoire de Physique Théorique et Hautes Energies is Laboratoire associé au Centre National de la Recherche Scientifique-URA 63. We thank the Institut du Développement et des Ressources en Informatique Scientifique (IDRIS) for allocation of computer time on the CRAY C-98. M.T.G. acknowledges partial financial support through the Portuguese government project, PRAXIS XXI/2/2.1/FIS/181/94. M.J.P.N. acknowledges the financial support of the EC through Grant No. ERBCHBGCT940721, while J.M.T. acknowledges the financial support of the Portuguese government under Grant No. PRAXIS XXI/BD/2818/94.

APPENDIX

In order to determine the Curie line Eq. (25) and the direction $\mathbf{v}$ over which βf is expanded, we calculated the elements of the stability matrix $\mathbf{M}$, with $H=0$ and $\eta_l=0$ $(l\neq 0)$, and found

$$\frac{\partial^2 \beta f}{\partial \rho^2}=\frac{\partial \beta f_{\text{HC}}}{\partial \rho^2}-u_0, \tag{A1}$$

$$\frac{\partial^2 \beta f}{\partial \rho \partial \eta_k}=0, \tag{A2}$$

$$\frac{\partial^2 \beta f}{\partial \eta_k \partial \eta_j}=\rho^2 u_k(\delta_{j,k}-\rho u_j\langle P_k P_j\rangle), \tag{A3}$$

where $\langle A(x)\rangle=(1/C)\int_{-1}^{1}A(x)\exp(\Sigma_{k=1}^{\infty}\rho\eta_k u_k P_k(x))$, with C given by Eq. (19). $\det\mathbf{M}=0$ has several types of solutions. A zero of Eq. (A1) corresponds to the isotropic critical point. Note that of the terms $\partial^2\beta f/\partial\eta_k^2$ that which vanishes at the lowest density corresponds to $k=1$ $[u_l(T)>u_{l+1}(T)$ for $l\geq 1]$, and thus the Curie line is given by $\rho u_1=3$. This line separates the (ρ,T) plane into two regions corresponding to ordered and disordered phases. The eigenvector associated with this zero eigenvalue of $\mathbf{M}$ is given by Eq. (26).

The expansion of βf along a line given by Eqs. (27) or (33) can be written as

$$\beta f(\rho_C+x_0\delta^2,\delta+x_1\delta^2,x_2\delta^2,\ldots)=\sum_{m=0}^{\infty}\frac{\delta^m}{m!}\Theta^m[\beta f], \tag{A4}$$

where ρ_C is the density of the Curie critical point, Eq. (28), or of the tricricritical point, Eq. (34), respectively. Θ^m is the mth power of the differential operator Θ,

$$\Theta=\delta\sum_{i=0}^{\infty}\left(x_i+\frac{\partial}{\partial\eta_i}\right)+\frac{\partial}{\partial\eta_1}. \tag{A5}$$

This expansion involves derivatives of βf with respect to ρ and each of the η_l. The derivatives are evaluated at $\eta_l=0$ $(l\neq 0)$. It is easily seen, after carrying out some of them, that they involve terms of the type

$$\langle P_l(x)P_k(x)\cdots P_n(x)\rangle. \tag{A6}$$

Using the recursion relation for the Legendre polynomials it is possible to convert the terms in Eq. (A6) in a sum of terms $\langle P_1(x)P_i(x)\rangle$, given by

$$\langle P_1(x)P_i(x)\rangle = \frac{i+1}{2i+1}\langle P_{i+1}(x)\rangle + \frac{i}{2i+1}\langle P_{i-1}(x)\rangle. \tag{A7}$$

It is easily seen that in the absence of a magnetic field,

$$\langle P_k(x)\rangle = \eta_k \quad (k\neq 0), \tag{A8}$$

and so the terms in the expansion (A4) are greatly reduced.

The coefficient of δ^3 in Eq. (A4) vanishes identically over the Curie line. The nonzero derivatives that appear in the δ^4 term are given by Eqs. (A1), (A3), and

$$\frac{\partial^3 \beta f}{\partial \eta_2 \partial \eta_1^2} = -\frac{2}{15}\rho^4 u_1^2 u_2, \tag{A9}$$

$$\frac{\partial^3 \beta f}{\partial \rho \partial \eta_1^2} = \rho u_1(2-\rho u_1), \tag{A10}$$

$$\frac{\partial^4 \beta f}{\partial \eta_1^4} = \frac{2}{15}\rho^5 u_1^4. \tag{A11}$$

The nonzero derivatives of the fifth order term are Eq. (A9) and

$$\frac{\partial^3 \beta f}{\partial \eta_1 \partial \eta_2 \partial \eta_3} = \frac{3}{35}\rho^4 u_1 u_2 u_3, \tag{A12}$$

$$\frac{\partial^3 \beta f}{\partial \rho \partial \eta_k^2} = 2\rho u_k - \frac{3\rho^2 u_k}{2k+1}, \tag{A13}$$

$$\frac{\partial^3 \beta f}{\partial \eta_1^3 \partial \eta_3} = -\frac{2}{35}\rho^5 u_1^3 u_3. \tag{A14}$$

Finally, the nonzero derivatives in the coefficient of δ^6 are Eqs. (A9), (A10), and

$$\frac{\partial^3 \beta f}{\partial \rho^3} = \frac{\partial^3 \beta f_{\mathrm{HC}}}{\partial \rho^3}, \tag{A15}$$

$$\frac{\partial^4 \beta f}{\partial \eta_1^2 \partial \eta_2^2} = -\frac{11}{105}\rho^5 u_1^2 u_2^2, \tag{A16}$$

$$\frac{\partial^4 \beta f}{\partial \rho \partial \eta_1^2 \partial \eta_2} = -\frac{8}{15}\rho^3 u_1^2 u_2, \tag{A17}$$

$$\frac{\partial^4 \beta f}{\partial \rho^2 \partial \eta_1^2} = 2u_1(1-\rho u_1), \tag{A18}$$

$$\frac{\partial^5 \beta f}{\partial \rho \partial \eta_1^4} = \frac{2}{3}\rho^4 u_1^4, \tag{A19}$$

$$\frac{\partial^5 \beta f}{\partial \eta_1^4 \partial \eta_2} = \frac{12}{175}\rho^6 u_1^4 u_2, \tag{A20}$$

$$\frac{\partial^6 \beta f}{\partial \eta_1^6} = -\frac{16}{63}\rho^7 u_1^6. \tag{A21}$$

[1] E. Lomba, J.J. Weis, N.G. Almarza, F. Bresme, and G. Stell, Phys. Rev. E **49**, 5169 (1994).

[2] M.J.P. Nijmeijer and J.J. Weis, Phys. Rev. Lett. **75**, 2887 (1995); Phys. Rev. E **53**, 591 (1996).

[3] J.M. Tavares, M.M. Telo da Gama, P.I.C. Teixeira, J.J. Weis, and M.J.P. Nijmeijer, Phys. Rev. E **52**, 1915 (1995).

[4] Although the magnetic interactions considered in this work are invariant under rotations both in the position and spin space, we call them anisotropic to be consistent with [3] and with the literature on liquid crystals.

[5] P.C. Hemmer and D. Imbro, Phys. Rev. A **16**, 380 (1977).

[6] A.Z. Panagiotopoulos, Molec. Sim. **9**, 1 (1992); B. Smit, in *Computer Simulation in Chemical Physics*, edited by M.P. Allen and D.J. Tildesley (Kluwer, Dordrecht, 1993).

[7] J.M. Kincaid, G. Stell, and E. Goldmark, J. Chem. Phys. **65**, 2172 (1976); J.M. Kincaid and G. Stell, *ibid.* **67**, 420 (1977).

[8] P. Bolhuis and D. Frenkel, Phys. Rev. Lett. **72**, 2211 (1994); P. Bolhuis, M. Hagen, and D. Frenkel, Phys. Rev. E **50**, 4880 (1994).

[9] P. Frodl and S. Dietrich, Phys. Rev. A **45**, 7330 (1992).

[10] K. Binder, Z. Phys. B **43**, 119 (1981).

[11] M.N. Barber, in *Phase Transitions and Critical Phenomena*, edited by C. Domb and J.L. Lebowitz (Academic Press, London, 1983), Vol. 8; *Finite Size Scaling and Numerical Simulation of Statistical Systems*, edited by V. Privman (World Scientific, Singapore, 1990).

[12] A.M. Ferrenberg and R.H. Swendsen, Phys. Rev. Lett. **63**, 1195 (1989); R.H. Swendsen, Physica A **194**, 53 (1993), R.H. Swendsen. J.S. Wang, and A.M. Ferrenberg, in *The Monte Carlo Method in Condensed Matter Physics*, edited by K. Binder, Springer Topics in Applied Physics Vol. 71, 2nd ed. (Springer, Berlin, 1995).

[13] U. Wolff, Phys. Rev. Lett. **62**, 361 (1989).

[14] J.M. Caillol, J. Chem. Phys. **98**, 9835 (1993).

[15] B. Widom, J. Chem. Phys. **39**, 2808 (1963).

[16] B. Smit and D. Frenkel, Mol. Phys. **68**, 951 (1989).

[17] G.L. Deitrick, L.E. Scriven, and H.T. Davis, J. Chem. Phys. **90**, 2370 (1989).

[18] K.K. Mon and K. Binder, J. Chem. Phys. **96**, 6989 (1992).

[19] I.D. Lawrie and S. Sarbach, in *Phase Transitions and Critical Phenomena*, edited by C. Domb and J.L. Lebowitz (Academic Press, London, 1984), Vol. 9.

[20] R. Evans, Adv. Phys. **28**, 143 (1979).

[21] J.-P. Hansen and I.R. McDonald, *Theory of Simple Liquids* (Academic, London, 1986).

[22] We note that det$\mathbf{M}>0$ is only a necessary condition for positive definiteness, since $\mathbf{M}$ is positive definite iff all principal determinants are positive.

[23] S. Krinsky and D. Mukamel, Phys. Rev. B **11**, 399 (1975).

[24] B. Groh and S. Dietrich, Phys. Rev. E **50**, 3814 (1994).

[25] N.B. Wilding and P. Nielaba, Phys. Rev. E **53**, 926 (1996).